Article

Testing of Newly Developed Wide-Field Dual-Array Suprachoroidal–Transretinal Stimulation Prosthesis in Dogs

Takeshi Morimoto[1], Takashi Fujikado[2], Hiroyuki Kanda[3], Tomomitsu Miyoshi[4], Takao Endo[5], Kentaro Nishida[1], Haruhiko Kishima[6], Toru Saito[7], Kunihiko Ito[7], Motoki Ozawa[7], and Kohji Nishida[5,8]

[1] Department of Advanced Visual Neuroscience, Graduate School of Medicine, Osaka University, Osaka, Japan
[2] Graduate School of Frontier Biosciences, Osaka University, Osaka, Japan
[3] Department of Applied Visual Science, Graduate School of Medicine, Osaka University, Osaka, Japan
[4] Department of Integrative Physiology, Graduate School of Medicine, Osaka University, Osaka, Japan
[5] Department of Ophthalmology, Graduate School of Medicine, Osaka University, Osaka, Japan
[6] Department of Neurosurgery, Graduate School of Medicine, Osaka University, Osaka, Japan
[7] NIDEK, Co., Ltd., Gamagori, Aichi, Japan
[8] Integrated Frontier Research for Medical Science Division, Institute for Open and Transdisciplinary Research Initiatives (OTRI), Osaka University, Osaka, Japan

Purpose: This study was conducted to investigate the feasibility of a newly developed wide-field dual-array suprachoroidal–transretinal stimulation (STS) prosthesis in dogs and to examine its biocompatibility and stability over a 4-month period.

Methods: Three types of STS dual arrays were designed and tested. The STS dual-array was implanted into a scleral pocket of the left eye of six healthy beagle dogs. Ophthalmic examinations, fundus photography, fluorescein angiography (FA), electroretinography (ERG), and functional testing of this system were conducted postoperatively. The dogs were euthanatized at the end of the experiment, and their eyes were enucleated and histologically examined.

Results: All prostheses were successfully implanted without complications, and no serious adverse event occurred during the postoperative period. Fundus photographs and FA showed no serious damage in the retina surrounding the arrays. The ERGs recorded from the implanted eyes showed no significant differences from those from control eyes. Histological evaluations demonstrated good preservation of the retina over the array. However, system failure occurred in 50% of the dogs owing to dog-specific habits.

Conclusions: Implantation of this prosthesis system in dogs is feasible and can be performed without significant damage to the eye. The biocompatibility and stability of the array were good during the observation period, but the low durability of the system against dogs (not humans) is an issue to be resolved in the future.

Translational Relevance: This study suggests that this wide-field dual-array prosthesis might widen the visual field and might be useful for patients with retinitis pigmentosa.

Introduction

Retinitis pigmentosa (RP) is a group of genetic diseases in which abnormalities of the photoreceptor or the retinal pigment epithelium of the retina lead to progression of vision loss.[1] RP affects more than 1.5 million individuals worldwide.[2]

Now there is still a lack of established therapy for treating or delaying the progression of RP. Consequently, patients with RP have little or no functional vision when they reach the final stage of the disease.

Retinal prostheses, as a replacement of photoreceptors, are implantable electric devices that electrically stimulate retinal neurons to evoke the light sensation "phosphene" to restore some vision in these patients.

The following three types of retinal prostheses have been devised, investigated, and clinically applied for blind patients with RP[3]: epiretinal,[4–7] subretinal,[8–11] and suprachoroidal.[12–16]

Our group developed the suprachoroidal–transretinal stimulation (STS) retinal prosthesis system, which is one of the suprachoroidal types. In this system, an electrode array is implanted into the deep sclera close to the choroid to reach the tip of electrode to the suprachoroidal zone,[17] and the return electrode is placed in the vitreous body.[16,18–21] Furthermore, we have conducted two clinical trials of an STS retinal prosthesis for blind patients with RP and confirmed the safety of this device and the restoration of some vision in these patients.[16,22,23] One of the problems of the application of retinal prostheses is that the prosthetic visual field provided by the retinal prostheses was very small, which was estimated to be approximately 15 degrees.[4–11,13,16] Visual field is important for patients with low vision to move freely. Some studies reported the presence of a significant correlation between the visual field and mobility performance in patients with RP with low vision.[24–26]

We and another research group investigated the effect of an expanded visual field in healthy participants using a retinal prosthesis simulator and documented that the wide visual field obtained by the retinal prosthesis simulator resulted in better mobility performance[27] or a significant improvement in visual acuity.[28] Thus, increasing the visual field would lead to improvement of the patient's vision.[29]

Therefore, we intended to proceed to a clinical trial by enlarging the size of the electrode array to expand the visual field. Increasing the size of the electrode array may raise some issues. One issue is that a large scleral incision is required and the array may not conform to the curvature of the eye.[29] Another issue is that a large array may result in mechanical damage during the operation and after the implantation.[30]

To address these issues, we recently developed a dual-array stimulation prosthesis covering a larger visual field and conforming to the curvature of the eye.

We conducted an acute animal experiment using this array and evaluated the surgical feasibility and safety of implantation of this dual-array STS prosthesis for 2 weeks.[31] Finally, we developed an implantable dual-array STS device that can be used for long-term implantation.

In this study, we explored the feasibility of the implantation, the suitability of the device for the tissue, and the biocompatibility and stability of the implanted devices through ophthalmic examinations, electrophysiological examinations, and histological analyses.

We herein demonstrate that our dual-array STS system can be implanted without complications and that the system is biocompatible and stable for long-term implantation.

Methods

Animals and Ethics Statement

Six adult male beagle dogs were used (Kitayama Labes Co., Ina, Japan). The age of the dogs was 8 to 13 months and they weighed 8 to 11 kg at the time of the implantation. All procedures were approved by the Animal Care and Use Committee of Osaka University (number: 26-013-005) and conformed to the ARVO statement on the Use of Animals in Ophthalmic and Vision Research. All procedures were performed under general anesthesia, all efforts were made to minimize potential suffering of the animals.

Wide-Field Dual-Array STS System

The wide-field dual-array STS system is manufactured by Nidek Co., Ltd. (Gamagori, Japan) and consists of an implanted system and an extracorporeal control system. The implanted component of the system consists of an extraocular microelectronic stimulator and a wide-field dual-electrode array (Fig. 1A–F).

The dual-array consists of a primary electrode array that is connected to a secondary electrode array with a lead wire. For this experiment, we designed three types of dual-array electrode. The type 1 system consisted of the dual-array (see Fig. 1A) and the scleral return electrode (0.5-mm diameter, 6-mm long platinum wire; see Fig. 1D). The size of both the primary and secondary arrays was 5.8 × 5.2 × 0.5 mm. Each array consisted of 25 platinum electrodes in a 5 × 5 arrangement fixed on a parylene substrate (30 μm).[32] The electrodes were made of 0.5-mm diameter bullet-type platinum, and the center-to-center separation of a pair of electrodes was 1.05 mm. The curvature of the electrode array was determined from a 23-mm sphere, as the mean diameter of the eyeball of adult Japanese people is approximately 23 mm. The multiplexer integrated circuit (MUX) was attached to the base of the main array and measured 5.8 × 5.0 mm. Details of the package of the MUX is shown in
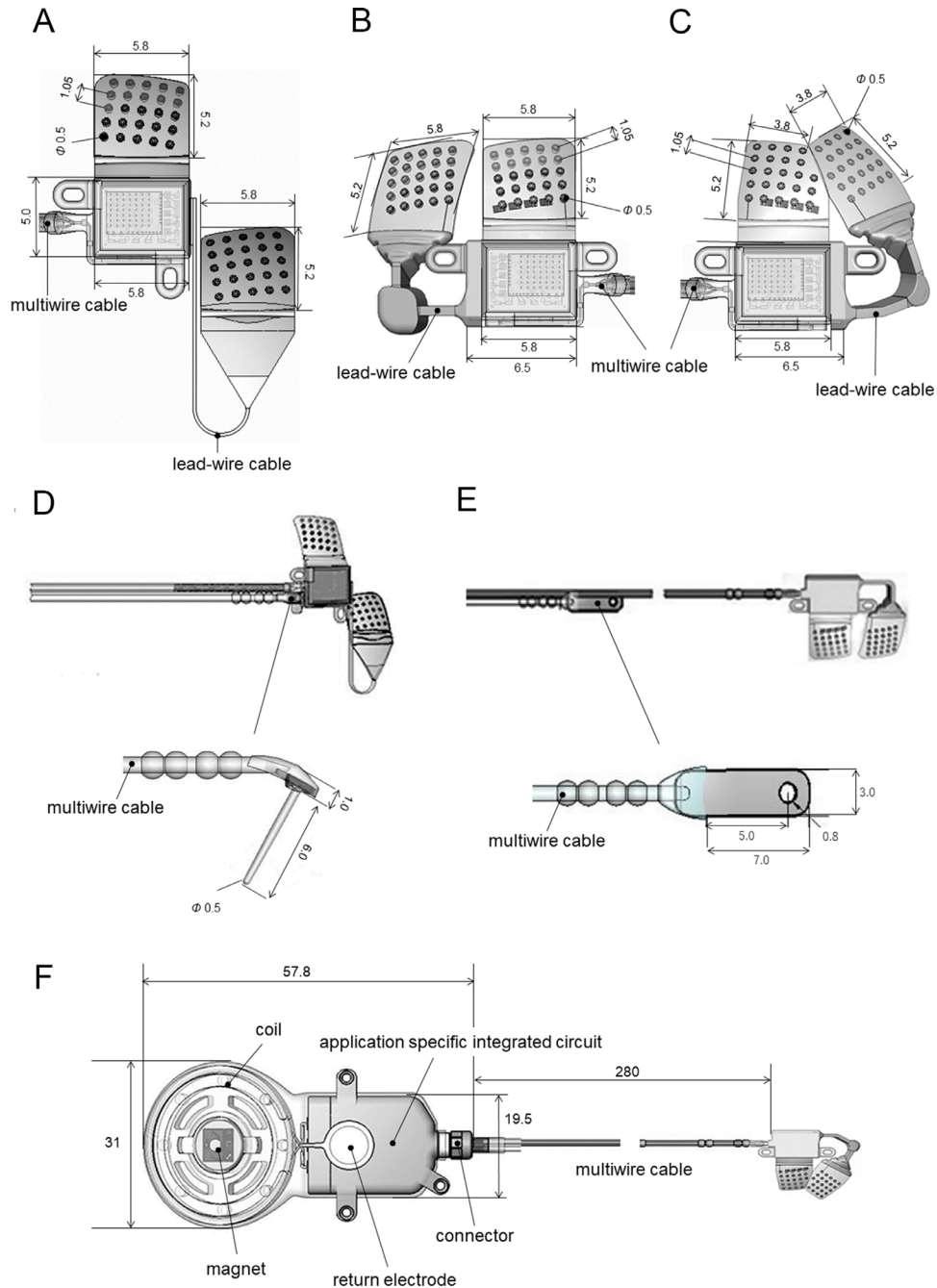
Figure 1. Illustration of the internal part of the wide-field dual-array suprachoroidal–transretinal stimulation (STS) system devices. The type 1 system consists of the dual-array and the scleral return electrode. (**A**) The size of both the primary and secondary arrays (dual arrays) was 5.8 × 5.2 × 0.5 mm with 25 platinum electrodes each fixed in a 5 × 5 arrangement. (**D**) The size of the scleral return electrode was a 0.5-mm-diameter, 6-mm-long platinum wire. The multiplexer IC (MUX) was attached to the base of the main array and measured 5.8 × 5.0 mm. The MUX was connected to the extraocular stimulator, whose size was approximately 57.8 × 31.0 × 6.5 mm (**F**), by a multiwire cable. The type 2 system consists of the dual-array (**B**) and the extraocular return electrode, which was a 3.0 × 5.0 × 0.3 mm platinum plate (**E**). The size and shape of the array were similar to those of type 1 array, although the lead wire connecting the primary array to the secondary array was changed **B**. The type 3 system consists of the dual-array without a return electrode. The shape of the dual-array was changed from quadrangle to trapezoid, the number of electrodes was decreased to 23 in the each of the arrays (**C**), the return electrode was removed, and the subdermal decoder package (as a return electrode) was set on the body of the extraocular stimulator.
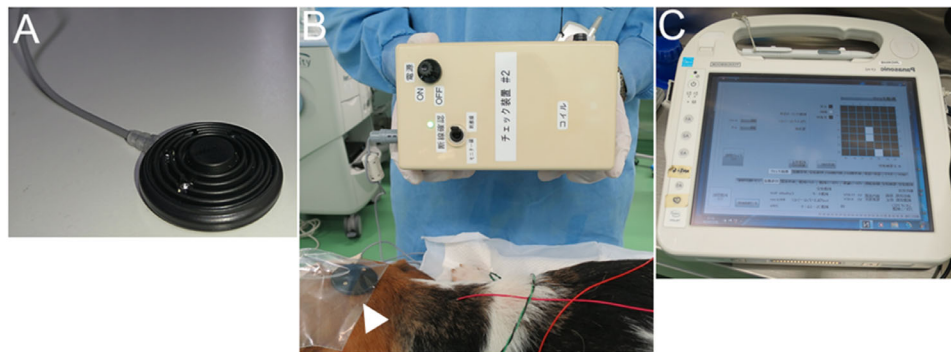
Figure 2. Photographs of the extracorporeal part of the STS system devices. The system consisted of a transmitter (**A**), a processor (**B**), and a personal computer (PC) (**C**). The stimulus sets were programmed using the technical computing software on a PC that sent the stimulus parameters to the processor. The signals and power information were then passed through the transmitter **B** (*white arrowhead*) to the subdermal microstimulator.

Supplementary Figure S1. The MUX was connected to the extraocular stimulator (see Fig. 1F) by a multiwire cable. Details of the connector are shown in Supplementary Figure S2. There are five wires in the connector (2 power wires and 3 signal wires). This connector is a screw type and is waterproof. The extraocular stimulator consists of an application-specific integrated circuit with a magnet and coil. This microelectronics receives signals and electric power from an external transmitter by electromagnetic induction and delivers them to the MUX through the multicable wire.

The type 2 system consisted of the dual-array (see Fig. 1B) and the extraocular return electrode ($3.0 \times 7.0 \times 0.3$ mm platinum plate; see Fig. 1E). The size and shape of the array were similar to those of the type 1 array; however, the lead wire connecting the primary array to the secondary array was changed. In the type 3 system, the shape of the dual-array was changed from quadrangle to trapezoid, the number of electrodes was decreased to 23 in each array (see Fig. 1E), the return electrode was removed, and another return electrode was set on the body of the extraocular stimulator (see Fig. 1F).

The extracorporeal component of the STS system consisted of a transmitter (Fig. 2A), a signal processor (Fig. 2B), and a personal computer (PC; Fig. 2C).

Anesthesia

The dogs were initially anesthetized intramuscularly using a mixture of 15 mg/kg ketamine HCl (Ketaral; Daiichi Sankyo Co., Ltd., Tokyo, Japan), 2 mg/kg xylazine (Seraktal; Bayer Health Care, Tokyo, Japan), and 0.2 mg/kg butorphanol (Betorphal; Meiji Seika Pharma, Co., Ltd., Tokyo, Japan), followed by an intraperitoneal injection of 0.05 mg/kg atropine

sulfate (Atropin; Mitsubishi Tanabe Pharma Corporation, Osaka, Japan). A tracheal tube was intubated and intravenous catheters were placed in the cephalic veins. The anesthesia was maintained using propofol (Rapinovet; Bayer HealthCare LLC, Leverkusen, Germany) at a dose of 6.0 mg/kg/h and a mixture of air/O_2 (2:1) and sevoflurane (Mylan; Pfizer Japan Inc., Tokyo, Japan) at an inspired concentration of approximately 2.0% with controlled ventilation. A heating pad was used to maintain body temperature at approximately 37°C. The electrocardiogram was continuously monitored, and the oxygenation of hemoglobin was monitored by pulse oximetry during surgery.

Surgical Procedure

Implantation was made to the left eye of each dog using the following surgical procedures: insertion of the dual-array into a deep lamellar scleral pocket, passing the cable into the head from the left orbit, and fixation of the extraocular stimulator on the surface of the left temporal muscle.

The conjunctiva was opened at the upper temporal quadrant near the limbus. A 15×7 mm scleral pocket was made at the temporal to upper temporal area 15 to 17 mm from the limbus (Fig. 3A). The dual-array was placed in the scleral pocket, and the multiplexer IC was sutured using 5–0 Dacron (Alcon, Fort Worth, TX, USA) and fixed on the sclera (Fig. 3B–D). The cable was then circled around the quadrant passing under the superior and lateral rectus muscles and sutured on the sclera (Figs. 3E, 3F). In the type 1 system, the return electrode was placed and sutured using 5–0 Dacron on the sclera at the upper nasal area. The tenon capsule and the conjunctiva were sutured
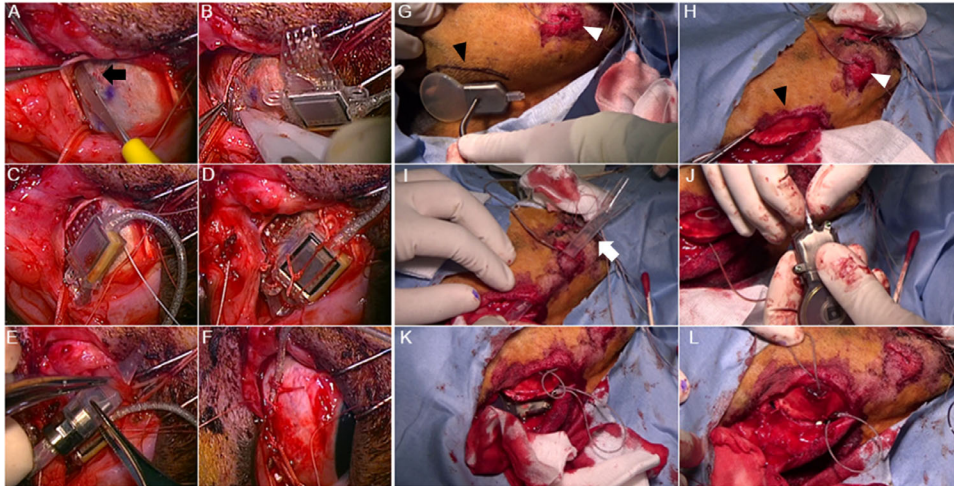
Figure 3. Photographs of implantation surgery. (**A**) Creation of a scleral pocket. (**B–D**) A dual-array is inserted into the scleral pocket and is sutured to the sclera. (**E, F**) A cable is passed under an extraocular muscle and is sutured to the sclera. (**G, H**) Skin incisions at the left brow (*white arrowhead*) and the temporal head (*black arrow*). (**I**) A cable is passed through a customized trocar (*white arrow*). (**J**) A cable is connected to an extraocular microstimulator. (**K, L**) Extraocular microstimulator implanted into the left temporal muscle and the muscle rift was sutured together.

using 8–0 Vicryl (Johnson & Johnson, New Brunswick, NJ, USA).

After the implantation of the array, a skin incision measuring approximately 3 cm was made at the left brow (Fig. 3G), and the subcutaneous tissue was prepared for inserting the cable. The cable was then passed from the left orbit to the brow incision through the periocular space using a customized trocar catheter (Medikit, Tokyo, Japan). In the type 2 system, the return electrode was placed and sutured using 5–0 Dacron on the surface of the frontalis muscle at this area.

A second skin incision was made sagittally between the median line and approximately 5 cm from the left ear (Figs. 3G, 3H). Then, the cable was passed from the first incision to the second incision under the skin using a longer customized trocar catheter (Medikit, Tokyo, Japan; Fig. 3I). Details of the connection between the stimulator and the cable are shown in Supplementary Figure S3. After connecting the cable to the microstimulator (Fig. 3J), the stimulator was placed in the left temporal muscle and tightly sutured using 0 silk (Alfresa Pharma Corporation, Osaka, Japan; Figs. 3K, 3L), and the skin incisions on the head and the brow were also sutured using 0 silk.

Ophthalmic Examinations

Each dog was subjected to comprehensive ophthalmic examinations (anterior segment and fundus examinations) before surgery, just after the surgery, and every month after until the end of the experiment.

Fundus Photography and Fluorescein Angiography

Color fundus photographs were taken while the dogs were under general anesthesia before surgery and every month after surgery. Fluorescein angiography (FA) was performed at 1, 3, and 6 months after surgery. For both procedures, the eyes were dilated using topical 2.5% phenylephrine hydrochloride and 0.5% tropicamide (Midrine P; Santen Co., Ltd., Osaka, Japan), and fundus photographs and FA were taken using a fundus camera (Retcam3; Clarity Medical Systems, Pleasanton, CA, USA). For FA, the photographs were taken after the injection of 0.075 mL/kg of 10% sodium fluorescein solution (Fluorescite; Alcon Japan Ltd., Tokyo, Japan) into a vein.

Electroretinography

Full-field electroretinograms (ERGs; scotopic rod response, bright flash [combined rod–cone], photopic cone response, and 30-Hz flicker) were recorded 1, 3, and 6 months after the implantation. While the dogs were under general anesthesia, the pupils were dilated using 2.5% phenylephrine hydrochloride and 0.5% tropicamide, and a 2.5% hydroxypropyl methylcellulose ophthalmic solution (Scopysol; Santen
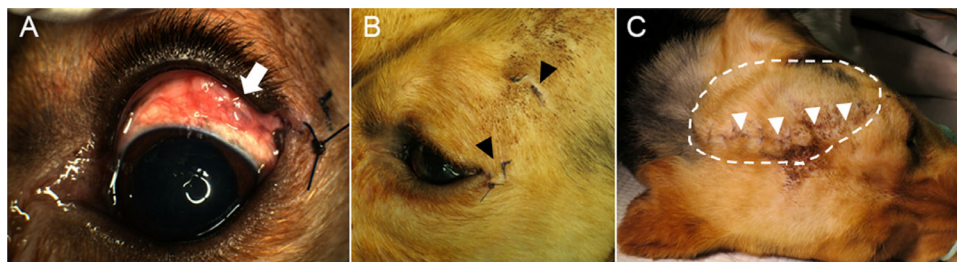
Figure 4. Photographs of dog no. 4 one month after implantation. (**A**) Anterior segment photography. Anterior segment photography reveals clear cornea and the conjunctival wounds (*white arrow*) healed properly, with no signs of infections. (**B**) Lateral view of dog. The position of the eye is orthophoric without proptosis, and the periorbital wounds healed properly (*black arrowheads*). (**C**) Top view of the dog head. The head wounds healed properly, and no sign of infections or wound dehiscence can be seen (*white arrowheads*). The position of the extraocular stimulator is indicated by the *circular white dot lines*.

Table 1. Summary of Experimental Results

No.	Array Type	Observation Period	Surgical Complication	Fundus	FA	ERG	Histology	Adverse Event	Functional Test	Cause of Failure
1	Type 1	4 mo	None	NP	NP	NP	NP	NP	Failure (IM)	Wire breakage
2	Type 1	4 mo	None	NP	NP	NP	NP	NP	Failure (3 mo)	wire breakage
3	Type 2	6 mo	None	Pigmentation	NP	NP	Choroid	Head wound dehiscence	Pass (6 mo)	
4	Type 2	6 mo	None	NP	NP	NP	NP	NP	Pass (6 mo)	
5	Type 3	6 mo	None	NP	NP	NP	NP	NP	Pass (6 mo)	
6	Type 3	6 mo	None	NP	NP	NP	NP	Head Wound dehiscence	Failure (3 mo)	Wire breakage

NP, not particular.

Co. Ltd., Osaka, Japan) was used with a corneal contact lens electrode/LED mini-Ganzfeld stimulator (WLS-20; Mayo Corporation, Nagoya, Japan). A reference electrode was inserted subdermally into the left ear, and a ground electrode was inserted subdermally into the nose. The animal was adapted to the dark for 30 minutes before the ERG recordings. ERGs were recorded from both eyes simultaneously according to International Society for Clinical Electrophysiology of Vision (ISCEV) standards. Responses elicited by the appropriate light stimuli were amplified, band-pass-filtered from 0.3 to 1000 Hz, and digitized at 3.3 kHz, which were averaged and analyzed using a computational ERG recording system (Neuropack; Nihon Kohden, Tokyo, Japan). A total of 4 to 20 responses were averaged with interstimulus intervals ranging from 0.5 to 10 seconds depending on the intensity of the stimulus.

ERG Analyses

The A-wave amplitudes were measured from the prestimulus baseline to the peak of the A-wave of the bright flash and cone ERGs, and the B-wave amplitude was measured from the trough of the A-wave to the peak of the B-wave of all ERGs. Data were analyzed using commercial software (JMP, version 14.0; SAS Institute Japan, Tokyo, Japan). Data are expressed as mean $\pm$ SD. To determine the significance of differences in the ERG amplitudes between operated eyes and unoperated fellow eyes, comparisons between the two groups were made using a paired *t*-test, when the data were normally distributed, or using the Mann–Whitney rank sum test, when the data were not normally distributed. A significance level of 0.05 was used in all analyses.

Functional Testing of the STS System

Functional testing of the STS system was performed to confirm its integrity and stability. At 1 and 3 months and at the end of the experiments (4–6 months) after implantation, the artifacts evoked by electrical stimulation were recorded using a contact lens corneal electrode (WLS-20). A reference electrode was inserted subdermally into the left ear, and a ground electrode was inserted subdermally into the nose. Cathodic-first biphasic pulses of 200 to 1000 µA were delivered with a duration of 0.5 ms/phase and a pulse duration of 0.5 ms. The frequency of the pulses was 20 Hz for 0.5 seconds.

The responses were amplified and band-pass-filtered from 0.3 to 1000 Hz, and the responses were
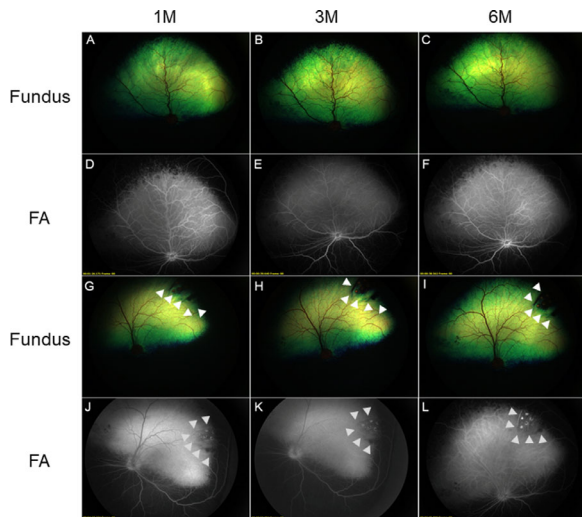
Figure 5. Fundus photographs and fluorescein angiograms 1, 3, and 6 months after implantation. Representative fundus photographs (**A–C**) and fluorescein angiographs (**D–F**) 1, 3, and 6 months after the implantation surgery. Fundus photographs showed that there were no ocular complications, infections, retinal detachment, or vitreous or subretinal hemorrhages. FA also demonstrated intact vasculature without signs of inflammation, leakage, obstruction, or formation of new vessels. Fundus photography (**G–I**) and FA (**J–L**) of dog no. 3. Fundus photographs showed retinal pigmentation 1 month after implantation; there is no severe retinal damage surrounding the area **G** (*white arrowheads*). Although FA showed the electrodes in the pigmented area, there is no severe retinal damage surrounding the array **J** (*gray arrowhead*). The size of the pigmented area remained unchanged throughout the experimental period (6 months) **G–I** (*white arrowheads*). FA also demonstrated no detectable signs of retinal damage, signs of inflammation, leakage, obstruction, or formation of new vessels in the pigmented area surrounding the array **J–L** (*gray arrowheads*).

digitized at 3.3 kHz and recorded using a computational ERG recording system (Neuropack).

Histological Analyses

At the end of the experiment, the animals were euthanatized using 120 mg/kg intravenous pentobarbital (Somunopentyl; Kyoritsu Seiyaku Corporation, Tokyo, Japan). Both eyes were enucleated, after which the array and cables were removed from the left eyes. The eyes were then placed in a Davidson's fixative solution[33] for 30 minutes at room temperature (RT). The eyes were trimmed, and the eyecups with the optic nerve were placed in 10% formalin in 0.1 M PB at 4°C for 24 hours. Tissues were trimmed and embedded in plastic. Semithin sections (4.0 μm) were cut along the meridian, including the optic disc and the scleral pocket, and stained with hematoxylin and eosin for examination by light microscopy.

Results

Results of Implantation Surgery and Postoperative Follow-Up Examinations

All devices were safely implanted, and no intraoperative complications were encountered. There was no severe bleeding during the creation of the scleral pocket. The dual-array electrode array could be easily inserted into the scleral pocket (see Figs. 3B–D), and the extraocular microstimulator was also placed into the temporal muscle without severe bleeding or damage (Fig. 3G–L). The mean (±SD) surgery time was 3.25 ± 0.49 hours (range = 2.43–3.75 hours). Just after implantation surgery, comprehensive ophthalmic examinations were performed to check for ocular damages, such as corneal damage, cataract, inflammation, vitreous hemorrhage, and retinal detachment.

One day after surgery, moderate edema and hematomas were observed in the periorbital and head regions. Conjunctival chemosis and injection were also observed in all cases. Approximately 1 week after surgery, the conjunctival chemosis, periorbital and head edema, and hematoma had almost completely resolved. Within 1 month after surgery, the conjunctival wounds healed properly with no signs of infections or wound dehiscence, and the cornea was kept clear after the surgery (Fig. 4A). The position of the eyes was maintained orthophoric without proptosis, and the periorbital and head skin wounds also healed properly 1 month after the surgery (Figs. 4B, 4C). All animals moved freely in their kennels and presented no apparent alterations in their behavior. Although the fixation of the extraocular microstimulator was also stable throughout the observation period in all cases, there was wound dehiscence on the head in two dogs (Nos. 3 and 6), which was treated appropriately. A summary of the results for each animal is shown in Table 1. The experimental period was divided into 4 and 6 months depending on the result of the functional test.

Postoperative Fundus Examination and FA

Representative fundus photographs and fluorescein angiographs taken 1 to 6 months after the implantation surgery are shown in Figures 5A to 5F. The fundus photographs revealed that there were no ocular complications, infections, retinal detachment, or vitreous or subretinal hemorrhages (seeFigs. 5A–C). FA also demonstrated intact vasculature with no signs of inflammation, leakage, obstruction, or formation of new vessels (see Figs. 5D–F).
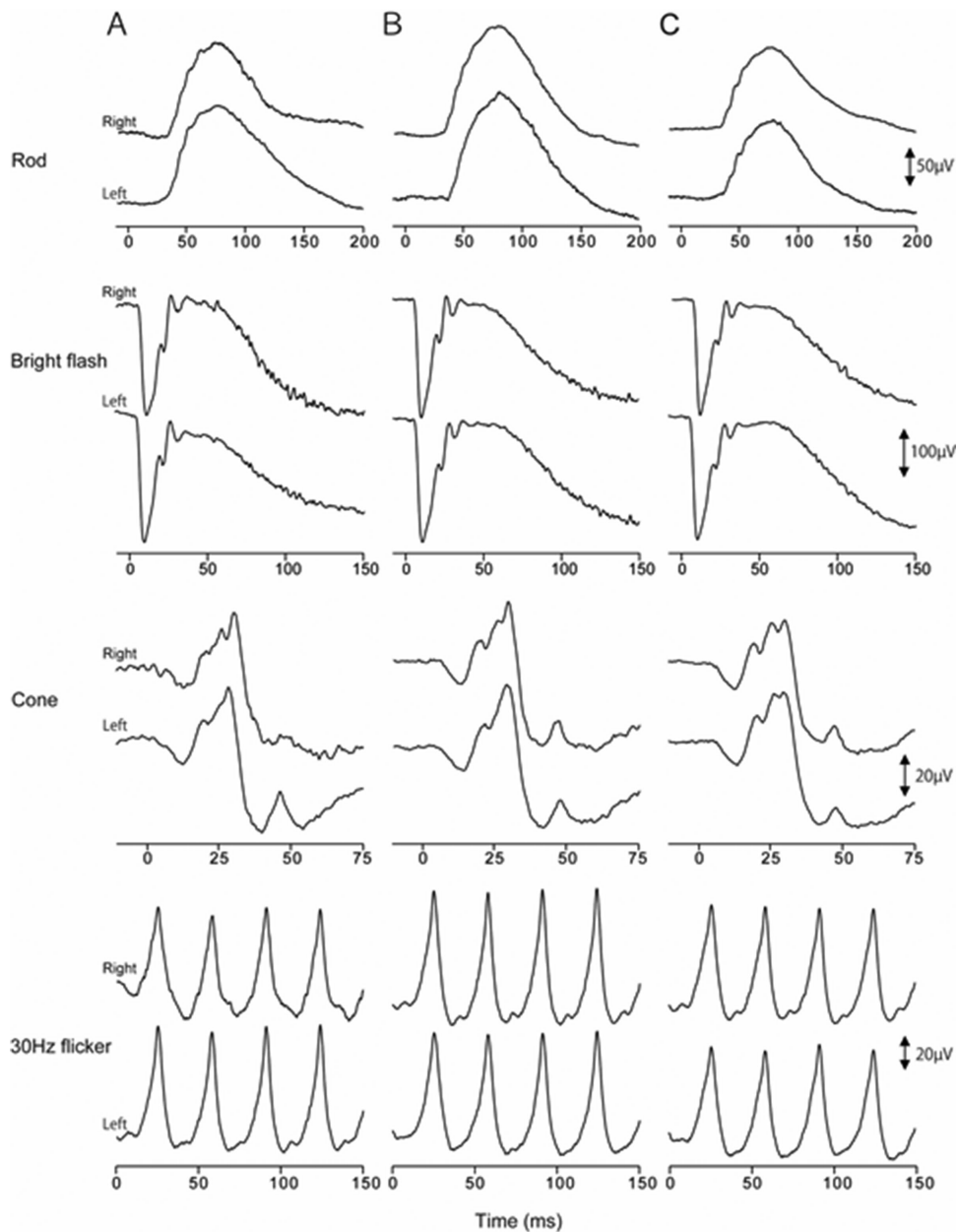
Figure 6. Representative four types of full-field ERG responses after the implantation surgery. Four types of representative ERG responses obtained from dog no. 3 (**A**) 1 month, (**B**) 3 months, and (**C**) 6 months after the implantation surgery. All ERGs had normal waves, and the wave shapes did not differ from those of ERGs recorded from the unoperated fellow eye at all time points after implantation. These results indicated that the function of rod and cone photoreceptors was not damaged by the implantation.

In only dog no. 3, the fundus photography images showed retinal pigmentation, which indicated the notch of the electrode array 1 month after implantation (Fig. 5G; white arrowheads), and FA revealed the electrodes in the pigmented area (Fig. 5J; gray arrowheads). However, the size of the pigmented area remained unchanged throughout the experimental period (6 months; Figs. 5G–I; white arrowheads). FA also demonstrated that there were no detectable signs of retinal damage, signs of inflammation, leakage,

obstruction, or formation of new vessels in the pigmented and the surrounding area (Figs. 5J–L; gray arrowheads).

Full-Field ERGs

Four types of representative ERG responses were obtained from dog no. 3 after the surgery, which are shown in Figures 6A to 6C. All responses had normal waves in both eyes, and the wave shapes did not differ

Table 2. Results of ERG Examinations in Dogs After Implantation Surgery

			1 mo (n = 6)			3 mo (n = 6)			6 mo (n = 6)		
			Implanted Eye	Fellow Eye	P Value*	Implanted Eye	Fellow Eye	P Value*	Implanted Eye	Fellow Eye	P Value*
Rod	B-wave	Amplitude, µV	104 ± 36.8	106 ± 37.6	0.1563	113 ± 24.0	119 ± 25.0	0.1563	110 ± 41.9	68.4 ± 6.64	–
		Implicit time, ms	68.4 ± 6.64	70.7 ± 6.91	0.625	68.4 ± 6.64	70.7 ± 6.91	0.3125	113 ± 44.3	70.7 ± 6.91	–
Bright flash	A-wave	Amplitude, µV	200 ± 40.6	182 ± 36.7	0.2188	193 ± 66.3	185 ± 58.3	0.4375	183 ± 53.1	169 ± 49.8	–
		Implicit time, ms	7.75 ± 0.52	8.50 ± 0.98	0.1250	7.90 ± 0.56	8.05 ± 0.48	1.000	8.32 ± 0.51	7.80 ± 0.42	–
	B-wave	Amplitude, µV	244 ± 40.8	237 ± 40.8	0.5625	238 ± 56.9	249 ± 56.9	0.2188	231 ± 36.6	221 ± 24.6	–
		Implicit time, ms	24.6 ± 1.35	24.3 ± 1.07	0.1250	24.8 ± 1.35	24.5 ± 0.59	0.750	26.5 ± 1.82	26.2 ± 1.63	–
Cone	A-wave	Amplitude, µV	11.2 ± 2.13	11.9 ± 4.07	0.8018	11.0 ± 1.90	10.3 ± 2.80	0.4375	9.51 ± 3.50	10.4 ± 1.76	–
		Implicit time, ms	11.3 ± 0.62	12.0 ± 1.13	0.2009	11.9 ± 0.98	11.8 ± 0.86	0.5761	12.2 ± 0.67	12.0 ± 0.60	–
	B-wave	Amplitude, µV	39.7 ± 5.79	39.8 ± 5.23	0.9427	41.1 ± 9.27	42.1 ± 10.6	0.3125	42.2 ± 12.8	29.4 ± 1.36	–
		Implicit time, ms	27.4 ± 2.38	28.8 ± 2.35	0.0625	28.8 ± 1.20	28.8 ± 1.20	1.000	43.3 ± 13.9	29.1 ± 1.45	–
30 Hz flicker	B-wave	Amplitude, µV	56.5 ± 9.20	57.8 ± 9.62	0.3125	63.6 ± 8.40	67.1 ± 10.9	0.0625	58.4 ± 5.60	63.0 ± 2.46	–
		Implicit time, ms	33.1 ± 0.58	32.9 ± 0.31	0.625	32.9 ± 0.15	33.2 ± 0.31	0.1438	33.0 ± 0.24	33.2 ± 0.30	–
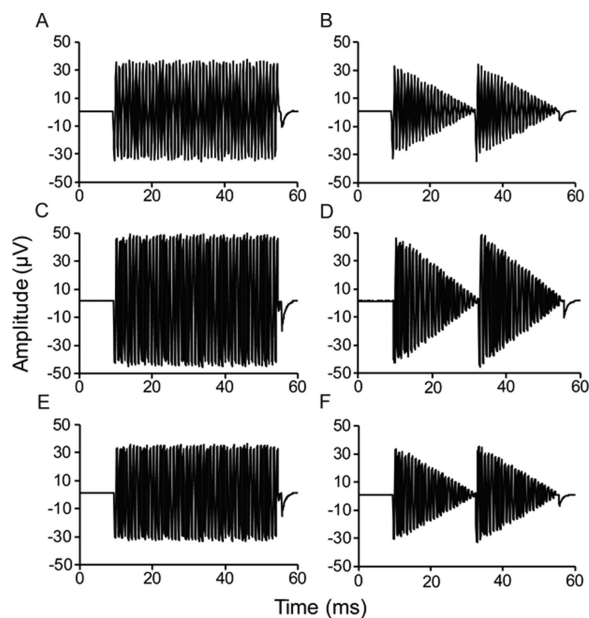
Figure 7. Representative stimulus artifact waveforms from 1 to 6 months after implantation surgery. Representative waveforms of the stimulus artifacts obtained from dog no. 4. Waveforms of artifacts derived from the dual-array sequentially, (**A**) 1 month, (**C**) 3 months, and (**E**) 6 months after implantation surgery. All electrodes could deliver the electric currents. Waveforms of artifacts evoked by pattern stimulation (**B**) 1 month, (**D**) 3 months, and (**F**) 6 months after implantation surgery. The amplitude of the artifacts was altered by the current intensity in each array.

from those of ERGs recorded from the unoperated fellow eye at all time points after implantation in all animals. No significant difference was observed in the amplitudes and in the implicit times between the operated eyes and the fellow eyes in all the four types of ERGs (Table 2).

These results indicated that the implantation did not damage the function of rod and cone photoreceptors.

Functional Testing of the STS System

Representative stimulus artifact waveforms at 1 to 6 months after the implantation surgery are shown in Figures 7A to 7F. All electrodes could deliver the electric currents (see Figs. 7A, 7C, 7E), and pattern stimulation could also be performed (see Figs. 7B, 7D, 7F). The amplitude of the artifacts was altered by the intensity of the current.

One animal (no. 1) failed the functional test at 1 month and 2 animals (nos. 2 and 6) failed the test at 3 months after the surgery, due to disconnection of the cable wires near the connector to the extraocular microstimulator (Figs. 8A–C; white line box and black dotted line box). However, three animals passed

the functional test at 6 months after the implantation surgery (see Table 1).

Histological Analyses

At the end of the experiments, the animals were deeply anesthetized and then euthanatized using an overdose of pentobarbital. The eyes were then enucleated. The fixation of the electrode array and the cable was examined macroscopically. Figures 9A to 9D show the representative photographs of the implanted eyes. The electrode array was found to be completely inserted into the scleral pocket and had not rotated on its axis (see Figs. 9A, 9B). Sections prepared from the implanted eyes revealed no obvious changes in the structure of the neural retina, retinal pigment epithelium (RPE) layer, and the choroid beneath the electrode array (see Figs. 9C, 9D).

Figures 9E and 9F shows the eyeball from dog no. 3, in which the retinal pigmentation near the array was detected funduscopically. In the area beneath the implanted array, the sclera was thinning and the choroid was exposed (see Fig. 9F; white arrowhead). Sections obtained from the eyes revealed that the choroidal architecture was destroyed by the deep insertion of the array, although the changes were limited to the surrounding of the array (see Fig. 9H; black arrowhead). However, no obvious damage, such as edema or retinoschisis, was found in the other regions of the retina beneath the array (see Figs. 9G, 9H). The architectures of the RPE layer and neural retina were intact.

Discussion

In this study, we implanted our newly developed dual-array STS system into beagle dogs and examined the feasibility of the implantation and the biocompatibility and stability of the implanted devices.

Our results demonstrated the possibility of implantation of this system into dogs without complications and that this system was biocompatible with the tissue over a period of 4 months, although 3 devices (50%) failed owing to disconnection of the cable wires.

Surgical Feasibility of Implanting Dual-Array STS Electrode

The implantation surgery was successful in all cases and resulted in stable placement of the arrays over the experimental period. We found that creating the single larger scleral pocket was easier than creating two divided scleral pockets, and it was easy to adjust the
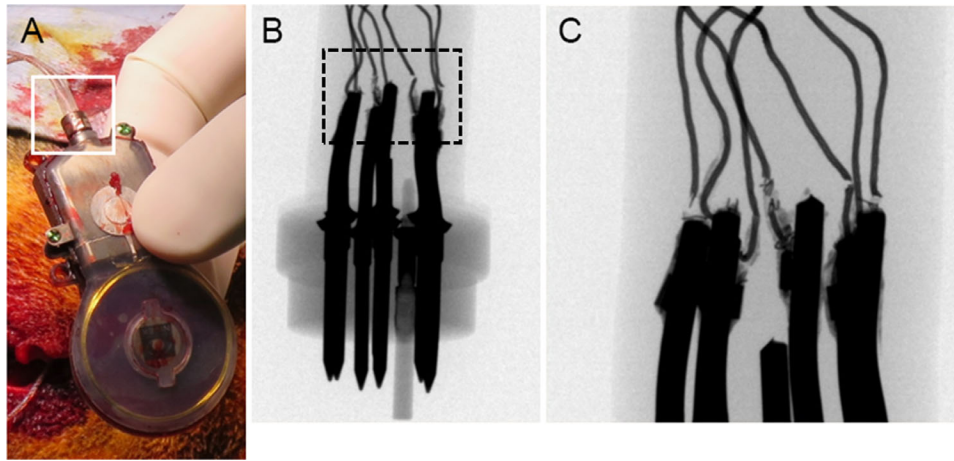
Figure 8. Photographs of the breakage of the cables in the failed device. (**A**) The failed microstimulator of dog no. 6, (**B**) the X-ray photograph of the cable wires near the connector, and (**C**) high magnification of the *black dotted line box*. The cable near the connection to the microstimulator was broken (*white line box*) and Xp showed the breakage of the cable wires (*black dotted line box*).

dual-array in the large scleral pocket. Furthermore, the position of the dual-array was stable and the arrays did not overlap and did not float up as they were equipped with bullet-shaped bulk electrodes.

In this study, we implanted three types of dual arrays into animals. Although there was no difference among the arrays in terms of the surgery, the type 3 dual-array might be suitable for implantation because the trapezoid shape of the array fitted better to the curvature of the eyeball.

## Biocompatibility and Stability of the Dual-Array STS System

Ophthalmic and histological examinations revealed no major adverse reactions in the retina beneath the wide-field dual-array during the experimental period. In dog no. 3, retinal pigmentation at the edge of the electrode array was observed postoperatively, but this pigmentation did not spread and did not lead to retinal degeneration. Histological examination of the eye of this dog revealed destruction of the choroid without retinal damage over the array due to the deep scleral insertion of the array to the outer choroid. This result indicated that it is important to control the depth of the scleral pocket to avoid choroidal damage.

In all animals, the ERG examinations also demonstrated no significant decline of retinal function in the implanted eyes than that in the control eyes, indicating good biocompatibility of the implanted system in dogs.

We also assessed the functional stability of this system to record the artifacts evoked by electrical pulses. Unfortunately, three animals did not pass the functional test within 3 months. The cause of system failure was the breakage of the cable proximal to the microstimulator in all three cases, although these cables passed the repeated bending test (47,000 cycles) before this experiment, and a similar type of microstimulator was used for implantation in 3 patients with RP for 1 year with no system failure in all the patients in the previous clinical trial.[16] In contrast, there was wound dehiscence on the heads in two dogs (nos. 3 and 6), which was treated appropriately, although no wound dehiscence was observed in all patients in the clinical trial. On the basis of these results, we assumed that the system failure and the wound dehiscence occurred due to the dogs' behaviors, such as scratching and shaking violently or hitting the head against the wall of the kennel, which are dog-specific habits (see Supplementary Materials). Therefore, it is unlikely that this system might fail when implanted in human patients.

In this study, we could not assess choroidal blood flow because we did not perform indocyanine green angiography. However, FA allowed us to know the status of the retinal circulation, retina, and RPE. As no abnormalities were observed, we believe that the choroidal circulation had no extensive impairment. Moreover, we did not examine the effect of the chronic stimulation by this system on the eyes to confirm its safety completely. With regard to the relationship between retinal damage and current intensity in the STS system, we reported that the threshold current for inducing retinal damage in rabbit eyes is greater than that required for eliciting phosphenes in human trials.[34,35] In the human trial of our system, we did not observe severe adverse effects, such as retinal degeneration.[16]
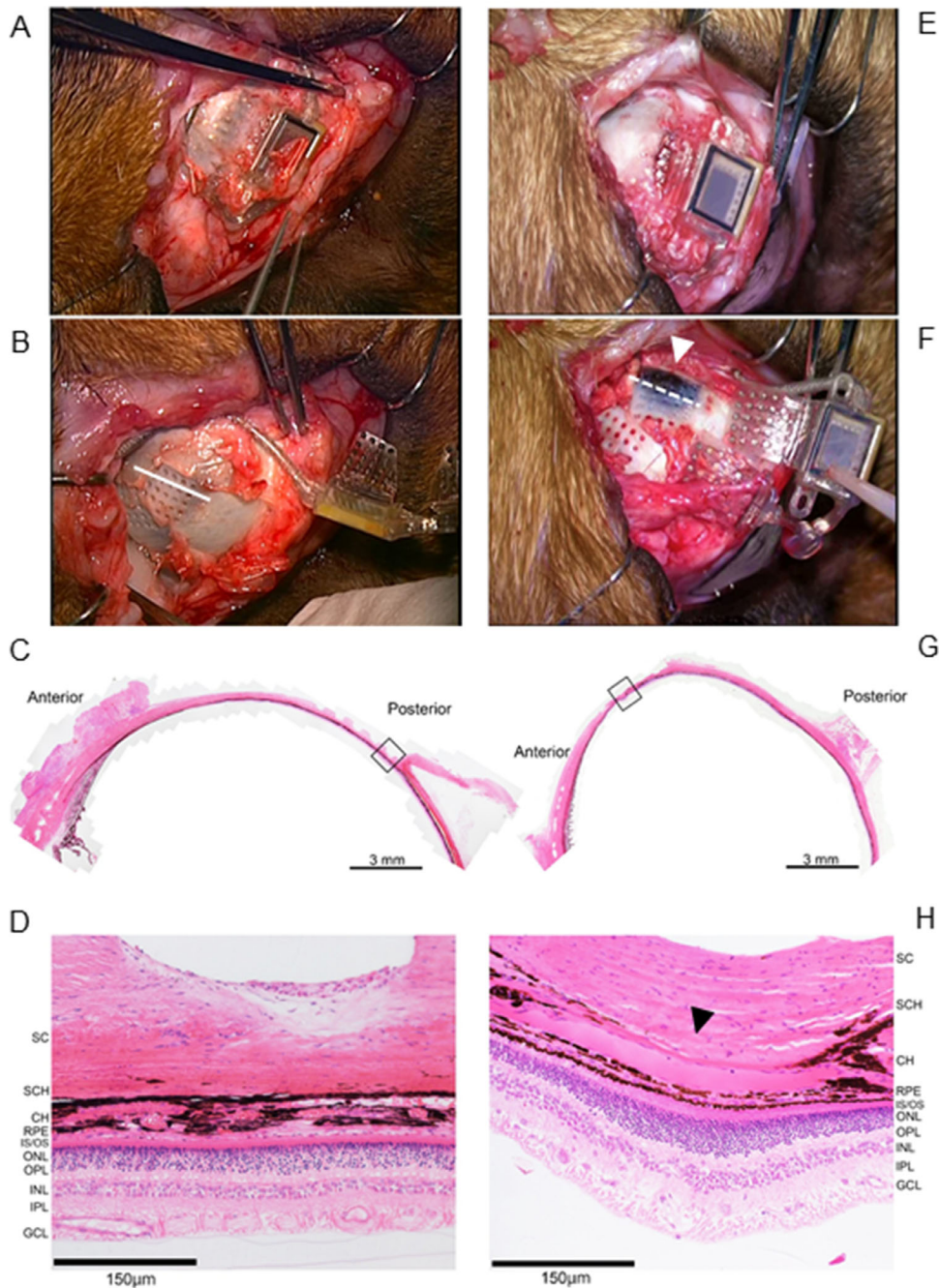
Figure 9. Surgical microscopic and light microscopic photographs of the implanted eyes. Surgical microscopic photographs of dog no. 5 (**A**) before and (**B**) after removal of the array. The electrode array was completely inserted into the scleral pocket and had not rotated on its axis. (**C, D**) Sections from the implanted eye **B** (*white line*). There is no obvious change in the structure of the retina and the choroid around the array. Magnifications: **C** × 100; and **D** × 400. Surgical microscopic photographs of dog no. 3 (**E**) before and (**F**) after removal of the array. Pathological changes were detected beneath the array **F** (*white arrowhead*). (**G, H**) Sections from the implanted eye **F** (*white dotted line*). Although the choroidal architecture surrounding the array was destroyed, no obvious damage was found in the other regions of the retina beneath the array (*black arrowhead*). Original magnifications: **G** × 100; and **H** × 400. CH, choroid; GCL, ganglion cell layer; INL, inner nuclear layer; IPL, inner plexiform layer; IS/OS, inner segments/outer segments of the photoreceptors; ONL, outer nuclear layer; OPL, outer plexiform layer; RPE, retinal pigment epithelium; SC, sclera; SCH, suprachoroid.

Considering these lines of evidence, this system might be safe under the same electric current used in the human trial.

Advantage of the Wide-Field Dual-Array STS System

Prosthetic visual acuity depends on the interelectrode distance. As the interelectrode distance of 700 μm on the human retina corresponds to a visual angle of approximately 2.4 degrees, the interelectrode distance of this array (1.05 mm) corresponds to a 2.36 logMAR visual acuity.[36] Wide-field dual-array causes expansion of the visual field and increases the number of electrodes compared with a single array, although the visual acuity of the wide-field dual-array is the same as that of a single array because the visual acuity depends on the interelectrode distance. The visual field significantly correlates with mobility performance in patients with RP with low vision.[24–26] It has been reported that a wide visual field obtained by the dual-array resulted in better mobility performance than that obtained by a single array in a retinal prosthesis stimulator study.[27–29]

The suprachoroidal location is more advantageous for the wide-field retinal prosthesis than other locations, such as epiretinal or subretinal location due to the need for a simple surgery and the low risk of surgical complications. The retinal prosthesis simulator study demonstrated that the superior location where the wide-field array was placed was better in improving mobility.[27]

We implanted our newly developed dual-array STS system into beagle dogs and determined the feasibility of the implantation and the biocompatibility and stability of the implanted devices.

Our results demonstrated that it is possible to implant the dual-array STS system into the deep lamellar scleral space of beagle dogs without complications and that the system was biocompatible with the tissue over a period of 4 months. However, 50% of the devices failed owing to disconnection of the cable wires; thus, the cables must be made more durable to solve this problem. These results indicate the possibility of implantation of a wider array as the next-generation STS system into human patients.

Acknowledgments

References

1. Hartong DT, Berson EL, Dryja TP. Retinitis pigmentosa. *Lancet*. 2006;368:1795–1809.
2. Daiger SP, Sullivan LS, Bowne SJ. Genes and mutations causing retinitis pigmentosa. *Clin Genet*. 2013;84:132–141.
3. Bloch E, Luo Y, da Cruz L. Advances in retinal prosthesis systems. *Ther Adv Ophthalmol*. 2019;11:2515841418817501.
4. Ho AC, Humayun MS, Dorn JD, et al. Long-term results from an epiretinal prosthesis to restore sight to the blind. *Ophthalmology*. 2015;122:1547–1554.
5. Luo YH, Zhong JJ, Clemo M, da Cruz L. Long-term repeatability and reproducibility of phosphene characteristics in chronically implanted Argus II retinal prosthesis subjects. *Am J Ophthalmol*. 2016;170:100–109.
6. da Cruz L, Dorn JD, Humayun MS, et al. Five-year safety and performance results from the Argus II retinal prosthesis system clinical trial. *Ophthalmology*. 2016;123:2248–2254.
7. Hornig R, Dapper M, Le Joliff E, et al. Pixium vision: first clinical results and innovative developments. In: Gabel VP, ed. *Artificial vision*. Cham: Springer, 2016; 99–113.

8. Zrenner E, Bartz-Schmidt KU, Benav H, et al. Subretinal electronic chips allow blind patients to read letters and combine them to words. *Proc Biol Sci.* 2011;278:1489–1497.

9. Stingl K, Schippert R, Bartz-Schmidt KU, et al. Interim results of a multicenter trial with the new electronic subretinal implant alpha AMS in 15 patients blind from inherited retinal degenerations. *Front Neurosci.* 2017;11:445.

10. Mandel Y, Goetz G, Lavinsky D, et al. Cortical responses elicited by photovoltaic subretinal prostheses exhibit similarities to visually evoked potentials. *Nat Commun.* 2013;4:1980.

11. Lorach H, Goetz G, Smith R, et al. Photovoltaic restoration of sight with high visual acuity. *Nat Med.* 2015;21:476–482.

12. Villalobos J, Nayagam DA, Allen PJ, et al. A wide-field suprachoroidal retinal prosthesis is stable and well tolerated following chronic implantation. *Invest Ophthalmol Vis Sci.* 2013;54:3751–3762.

13. Ayton LN, Blamey PJ, Guymer RH, et al. First-in-human trial of a novel suprachoroidal retinal prosthesis. *PLoS One.* 2014;9:e115239.

14. Petoe MA, McCarthy CD, Shivdasani MN, et al. Determining the contribution of retinotopic discrimination to localization performance with a suprachoroidal retinal prosthesis. *Invest Ophthalmol Vis Sci.* 2017;58:3231–3239.

15. Abbott CJ, Nayagam DAX, Luu CD, et al. Safety studies for a 44-channel suprachoroidal retinal prosthesis: a chronic passive study. *Invest Ophthalmol Vis Sci.* 2018;59:1410–1424.

16. Fujikado T, Kamei M, Sakaguchi H, et al. One-year outcome of 49-channel suprachoroidal-transretinal stimulation prosthesis in patients with advanced retinitis pigmentosa. *Invest Ophthalmol Vis Sci.* 2016;57:6147–6157.

17. Moisseiev E, Loewenstein A, Yiu G. The suprachoroidal space: from potential space to a space with potential. *Clin Ophthalmol.* 2016;10:173–178.

18. Kanda H, Morimoto T, Fujikado T, Tano Y, Fukuda Y, Sawai H. Electrophysiological studies of the feasibility of suprachoroidal-transretinal stimulation for artificial vision in normal and RCS rats. *Invest Ophthalmol Vis Sci.* 2004;45:560–566.

19. Nishida K, Kamei M, Kondo M, Sakaguchi H, Suzuki M, Fujikado T, Tano Y. Efficacy of suprachoroidal-transretinal stimulation in a rabbit model of retinal degeneration. *Invest Ophthalmol Vis Sci.* 2010;51:2263–2268.

20. Morimoto T, Kamei M, Nishida K, et al. Chronic implantation of newly developed suprachoroidal-transretinal stimulation prosthesis in dogs. *Invest Ophthalmol Vis Sci.* 2011;52:6785–6792.

21. Fujikado T, Kamei M, Sakaguchi H, et al. Feasibility of 2nd generation STS retinal prosthesis in dogs. *Conf Proc IEEE Eng Med Biol Soc.* 2013;2013:3119–3121.

22. Fujikado T, Kamei M, Sakaguchi H, et al. Testing of semichronically implanted retinal prosthesis by suprachoroidal-transretinal stimulation in patients with retinitis pigmentosa. *Invest Ophthalmol Vis Sci.* 2011;52:4726–4733.

23. Endo T, Fujikado T, Hirota M, Kanda H, Morimoto T, Nishida K. Light localization with low-contrast targets in a patient implanted with a suprachoroidal-transretinal stimulation retinal prosthesis. *Graefes Arch Clin Exp Ophthalmol.* 2018;256:1723–1729.

24. Szlyk JP, Fishman GA, Alexander KR, Revelins BI, Derlacki DJ, Anderson RJ. Relationship between difficulty in performing daily activities and clinical measures of visual function in patients with retinitis pigmentosa. *Arch Ophthalmol.* 1997;115:53–59.

25. Haymes S, Guest D, Heyes A, Johnston A. Mobility of people with retinitis pigmentosa as a function of vision and psychological variables. *Optom Vis Sci.* 1996;73:621–637.

26. Szlyk JP, Seiple W, Fishman GA, Alexander KR, Grover S, Mahler CL. Perceived and actual performance of daily tasks: relationship to visual function tests in individuals with retinitis pigmentosa. *Ophthalmology.* 2001;108:65–75.

27. Endo T, Hozumi K, Hirota M, Kanda H, Morimoto T, Nishida K, Fujikado T. The influence of visual field position induced by a retinal prosthesis simulator on mobility. *Graefes Arch Clin Exp Ophthalmol.* 2019;257:1765–1770.

28. Hayes JS, Yin VT, Piyathaisere D, Weiland JD, Humayun MS, Dagnelie G. Visually guided performance of simple tasks using simulated prosthetic vision. *Artif Organs.* 2003;27:1016–1028.

29. Ameri H, Ratanapakorn T, Ufer S, Eckhardt H, Humayun MS, Weiland JD. Toward a wide-field retinal prosthesis. *J Neural Eng.* 2009;6:035002.

30. Villalobos J, Allen PJ, McCombe MF, et al. Development of a surgical approach for a wide-view suprachoroidal retinal prosthesis: evaluation of implantation trauma. *Graefes Arch Clin Exp Ophthalmol.* 2012;250:399–407.

31. Lohmann TK, Kanda H, Morimoto T, et al. Surgical feasibility and biocompatibility of wide-field dual-array suprachoroidal-transretinal stimulation prosthesis in middle-sized animals. *Graefes Arch Clin Exp Ophthalmol.* 2016;254:661–673.

translational vision science & technology

32. Terasawa Y, Tashiro H, Nakano Y, et al. Mechanical machining-based three-dimensional electrode array for chronic neural stimulation. *Adv Biomed Eng*. 2016;5:137–141.

33. Tokuda K, Baron B, Kuramitsu Y, et al. Optimization of fixative solution for retinal morphology: a comparison with Davidson's fixative and other fixation solutions. *Jpn J Ophthalmol*. 2018;62:481–490.

34. Kanda H, Nakano Y, Terasawa Y, Morimoto T, Fujikado T. The relationship between retinal damage and current intensity in a pre-clinical suprachoroidal-transretinal stimulation model using a laser-formed microporous electrode. *J Neural Eng*. 2017;14:056013.

35. Terasawa Y, Tashiro H, Nakano Y, et al. Safety assessment of semichronic suprachoroidal electrical stimulation to rabbit retina. *Annu Int Conf IEEE Eng Med Biol Soc*. 2013;2013:3567–3570.

36. Kanda H, Morimoto T, Fujikado T, et al. Electrophysiological studies of the feasibility of suprachoroidal-transretinal stimulation for artificial vision in normal and RCS rats. *Invest Ophthalmol Vis Sci*. 2004;45:560–566.

Supplementary Materials

Supplementary Movie.   This video shows dog No. 6 scratching its head with its right hind leg at night. We believe that the act of scratching the head might have caused the head wound dehiscence and damage to the stimulator.

translational vision science & technology